Optimization of Solubility, Film Morphology and Photodetector Performance by Molecular Side-Chain Engineering of Low-Bandgap Thienothiadiazole-Based Polymers

Ji Qi, Xiaokang Zhou, Dezhi Yang, Wenqiang Qiao, Dongge Ma, and Zhi Yuan Wang**

A series of donor–acceptor (D-A) type low-bandgap polymers containing the terthiophene and thieno[3,4-*b*]thiadiazole units in the main chain but different numbers of identical side chains are designed and synthesized in order to study the effect of side chain on the polymer properties and optimize the performance of polymer photodetectors. Variation in the side chain content can influence the polymer solubility, molecular packing, and film morphology, which in turn affects the photodetector performance, particularly with regard to the photoresponsivity and dark current. X-ray diffraction patterns indicate that molecular ordering increases with more side chains. Atomic force microscopy shows that appropriate morphology of the active layer in the polymer photodetector is necessary for high photocurrent and low dark current. Using BCP as a hole blocking layer (10 nm), the photodetector based on P4 exhibits the optimized performance with specific detectivity of 1.4×10^{12} Jones at 800 nm, which is among the best reported values for polymer photodetectors and even comparable to that of a silicon photodetector.

1. Introduction

A variety of π-conjugated polymers have been explored for applications in optoelectronic devices such as light-emitting diodes, field-effect transistors, photovoltaic cells and photodetectors.[1–4] The properties of conjugated polymers, such as energy level, molecular stacking, carrier transport characteristics and solubility, are greatly affected by manipulation of the main-chain and side-chain structures.[5–12] A good solubility in common solvents is ideal for conjugated polymers to be used in devices and enables roll-to-roll, screen and ink jet printing, and other low-cost fabrication processes.[13–16] Having good solubility and satisfactory device performance is critically important for polymer optoelectronic materials to be used for solution-processed large-scale device applications. Side chains on conjugated polymers can directly affect the solubility and also play a multifunctional role in modulating the molecular energy level, solid state packing and film morphology, which all have significant impact on device performance. A flexible, long or bulky side chain is often introduced to impart solubility to conjugated polymers. In addition, subtle changes in the side chain can dramatically influence the aggregation behavior of conjugated polymers in the solid state, in particular with regard to their molecular stacking and film morphology, which are extraordinarily important for device application but usually difficult to predict.[17–21]

The influence of side chains on polymer property and device performance has largely been overlooked and less studied.[3,22] Recent studies show that the effect of side chains on the polymer properties, not just solubility, can be very significant, and sometimes even unexpected.[23–26] The studies on the effect of side chains typically involves the selection of chain type, size and location, but usually without guidelines and lack of a comprehensive understanding.[27–29] Therefore, systemic investigations into the structure-property relationship are required, especially for some conjugated polymers that are promising for use in optoelectronic devices in order to optimize the device performance.[30–34]

One of such polymers is poly[5,7-bis(2-thienyl)-thieno(3,4-*b*) diathiazole-thiophene-2,5] (PDDTT), as it has been successfully used in polymer photodetectors with high detectivity in a broad spectral region.[35–37] The low solubility of PDDTT in common organic solvents implies a potential for side-chain engineering, which may lead to changes in solubility and film morphology and subsequent optimization of photodetector performance.[38,39] In this work, we chose the PDDTT analogs having the terthiophene and thienothiadiazole (TT) units in the main chain and the dodecyl group on the side chain (**Scheme 1**). If different numbers of dodecyl groups are introduced, the polymer properties such as solubility, absorption, energy level, molecular stacking and film morphology are expected to change, which may lead to further optimization of polymer photodetectors.[40]

J. Qi, X. Zhou, Dr. D. Yang, Prof. W. Qiao,
Prof. D. Ma, Prof. Z. Y. Wang
State Key Laboratory of Polymer Physics and Chemistry
Changchun Institute of Applied Chemistry
Chinese Academy of Sciences
Changchun 130022, P. R. China
E-mail: wqqiao@ciac.ac.cn; wayne_wang@carleton.ca
J. Qi, X. Zhou
University of Chinese Academy of Sciences
Beijing 100049, P. R. China
Prof. Z. Y. Wang
Department of Chemistry
Carleton University
1125 Colonel By Drive, Ottawa, Ontario, Canada, K1S 5B6

DOI: 10.1002/adfm.201401948

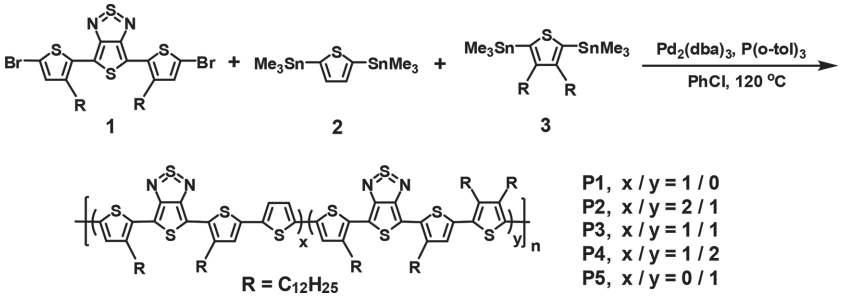

Scheme 1. Synthesis of polymers **P1**-**P5**.

2. Results and Discussion

2.1. Synthesis and Characterization

We carried out the Stille cross-coupling polymerizations of three monomers, 2,5-bis(5-bromo-3-dodecyl-2-thienyl)thieno[3,4-*b*][1,2,5]thiadiazole (monomer **1**), 2,5-bis(trimethylstannyl) thiophene (monomer **2**) and 2,5-bis(trimethylstannyl)-3,4-bisdodecyl thiophene (monomer **3**) in different molar ratios and obtained five polymers (**P1**-**P5**, Scheme 1) with different numbers of pendent dodecyl groups. The side-chain content in polymer is readily adjusted by varying the ratios of monomers **2** and **3** in polymerization. Herein, if assuming the segment (*x*) derived from monomers **1** and **2** as a base polymer without side chains and the segment (*y*) derived from monomers **1** and **3** as the side-chain block that is to be introduced into the base polymer, the side-chain content (*A*) in polymers **P1**-**P5** can be defined as $A = y/(x+y)$. The actual *x* and *y* or *x*/*y* ratios could be estimated from the ^{1}H NMR data of the polymers and details are given in Supporting Information (SI). Accordingly, the side-chain content of **P1**-**P5** gradually increases in order of 0%, 41%, 49%, 63% and 100%, respectively. The actual side-chain contents match well with those in feed, namely 0%, 33%, 50%, 67% and 100% for **P1**-**P5**, respectively.

All the polymers were washed with aqueous sodium diethyldithiocarbamate to remove residual palladium as previously reported.[41] Detail syntheses and characterizations of the monomers and intermediate compounds are given in SI. The molecular weights of polymers **P1**-**P5** were measured by gel permeation chromatography. The number-average molecular weights (M_n) and polydispersity indices (PDI) are in the range of 9–14 kDa and 1.4–1.7, respectively (**Table 1**). To minimize the effect that molecular weight may have on the study, we selected the polymers with similar molecular weights.[42,43] The onset temperatures (T_d) for 5% weight loss of the polymers are above 300 °C in nitrogen and analysis by differential scanning calorimetry (DSC) indicates no thermal transitions for all the polymers (Figures S1 and S2).

2.2. Optical and Electrochemical Properties

The absorption spectra of the polymers in chlorobenzene and as thin films spin-coated on quartz substrate are shown in **Figure 1**, and the related data are listed in **Table 2**. All the polymers show broad and featureless absorption in the UV–Vis–NIR spectral region in solution and as thin film. In comparison with other polymers, **P5** with 100% side-chain content exhibits the maximal absorption at the shortest wavelength (723 nm) in solution, presumably due to its highly twisted main-chain structure.[44] A red-shift of more than 50 nm for the long wavelength absorption is observed for the films of all the polymers, owing to molecular ordering and stacking.[45] In particular, a significant red-shift of 102 nm was observed for the film of **P5**, which is probably due to some highly ordered structures, as also indicated by the increased intensity of the X-ray diffraction (XRD) peak (**Figure 2**). The half bandwidth of the absorption peaks in solution become narrower going from **P1** to **P5**, but is less pronounced for the polymer films. Thus, it seems that side-chain contents in these polymers affect their molecular ordering significantly, especially for the lamellar structure governed mainly by side-chain packing.[46,47]

Cyclic voltammetry (CV) was employed to examine the electrochemical properties of the polymers. The polymer films on the platinum electrode undergo reversible oxidation and irreversible reduction in acetonitrile, showing a larger oxidation current than reduction current. The highest occupied molecular orbital (HOMO) and lowest unoccupied molecular orbital (LUMO) energy levels are determined from the onset potentials of the first oxidation and reduction peaks, respectively (Figure S3). The LUMO energy levels are estimated to be −3.5 to −3.6 eV (Table 2), which are adequate for exciton dissociation with regard to that of PCBM (−4.2 eV).[48] The HOMO energy levels of **P1**-**P4** are calculated to be between −4.8 and

Table 1. Characterization of Polymers **P1**-**P5**.

Polymer	Side-chain Content (*A*)		M_n[b] [kDa]	M_w[b] [kDa]	PDI[b]	T_d[c] [°C]
	in feed [%]	in polymer[a] [%]				
P1	0	0	9.5	15.3	1.61	342
P2	33	41	11.2	17.2	1.54	349
P3	50	49	13.6	20.2	1.49	355
P4	67	63	13.0	19.2	1.48	365
P5	100	100	11.8	17.0	1.44	354

[a]Obtained from the NMR data; [b]Determined by GPC relative to polystyrene standards; [c]Onset temperature for 5% weight loss in nitrogen by TGA.

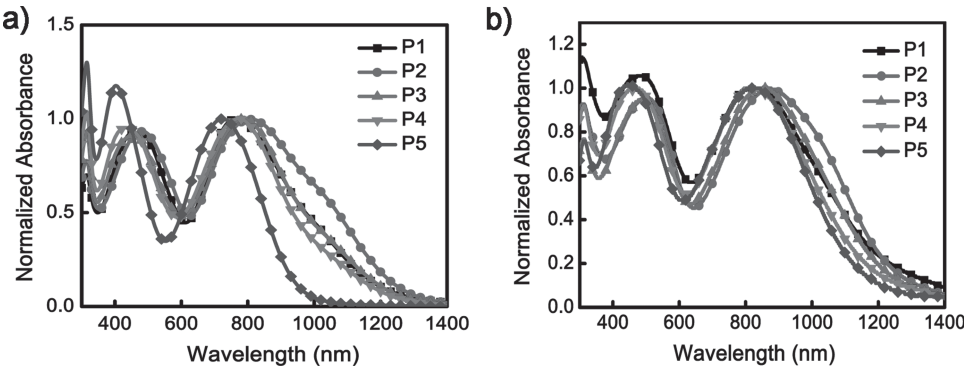

Figure 1. Absorption spectra of the polymers a) in chlorobenzene (at a concentration of 0.05 g/L) and b) as thin films spin-coated on quartz plate.

–4.9 eV, while **P5** shows a slightly lower HOMO energy level (–5.14 eV). Clearly, the HOMO energy levels are influenced by the alkyl side chains and become lower with a higher content of side chains. The conformational distortion is caused by steric hindrance due to the presence of side chain, which disrupts the π–π interaction and lowers the HOMO energy level.[21,49] The electrochemical bandgap values (E_g^{EC}) obtained from CV data are larger than the optical bandgaps (E_g^{opt}), which is in agreement with the previously reported data.[19,50]

2.3. Solubility and Molecular Stacking

The introduction of long alkyl side chains are expected to impact the solubility of polymers and at the same time affect molecular stacking and film morphology.[8,29] Polymers **P1**-**P5** are soluble in common organic solvents such as chloroform, chlorobenzene (CB) and 1,2-dichlorobenzene (DCB). As expected, polymers with more side chains are more soluble quantitatively than those with less ones. For example, the 100% side-chain polymer **P5** is readily soluble in chloroform with a concentration of 20 mg/mL at room temperature, while **P1** with 0% side-chain content could only be dissolved in hot DCB in a concentration of less than 10 mg/mL. As shown in Figure 2, the relative solubility of **P1**-**P5** in CB (10 mg/mL), after being heated at 80 °C for 2 h, can be visually distinguished. The solutions of **P1**-**P3** clearly show some undissolved particles and the solutions of **P4**-**P5** are completely clear and homogeneous. Thus, incorporation of a large number of side chains in conjugated polymers can effectively weakens the interchain interaction in solution and enables a higher solubility and feasible solution processability.[29,51]

The effect of side chains on the polymer morphology in the solid film state was then probed by XRD. The XRD peaks for **P2**-**P5** are located at 2θ = 9.24°, 7.04°, 5.14° and 3.40°, corresponding to *d*-spacing of 9.6, 12.5, 17.2 and 26.0 Å, respectively. As shown in Figure 2, **P1** appears to be amorphous and the diffraction peak of the polymer films becomes more intensively with an increase of side-chain content from 41% to 100%, along with the increased *d*-spacing and reduced half peak width. Therefore, the side-chain content does influence greatly the polymer stacking.[52,53] With an increase in the number of side chains, the intermolecular distance increases and the molecular stacking becomes more uniform. These results correlate well with the optical property of these polymers.

For device applications, the film quality such as surface roughness is particularly important.[21,54] The film roughness is related to the solubility of polymers and usually becomes smooth if the polymer is more soluble. From the atomic force microscopy (AFM) images of the pristine polymer films (Figure 2), the root-mean-square (RMS) roughness of the films of **P1**-**P5** are measured to be 3.27, 2.46, 1.57, 0.95 and 0.43 nm, respectively. Thus, polymers **P4** and **P5** with more dodecyl groups are able to form smooth films.

2.4. Fabrication and Characterization of Polymer Photodetectors

Ideally, a polymer with good solubility is used for device application and also leads to the device with the optimal performance. However, in most cases, the outcome is less satisfactory and

Table 2. Optical and Electrochemical Properties of Polymers **P1**-**P5**.

polymer	$\lambda_{max}^{soln.}$ [nm][a]	λ_{max}^{film} [nm][b]	$\Delta\lambda_{max}$ [nm][c]	E_g^{opt} [eV][d]	HOMO [eV][e]	LUMO [eV][e]	E_g^{EC} [eV][f]
P1	766	825	59	1.02	–4.83	–3.62	1.21
P2	812	873	61	1.01	–4.88	–3.55	1.33
P3	788	852	64	1.04	–4.90	–3.54	1.34
P4	771	828	57	1.07	–4.90	–3.54	1.36
P5	723	825	102	1.10	–5.14	–3.55	1.59

[a]Measured in chlorobenzene at a concentration of 0.05 g/L; [b]Film spin-cast from 10 mg/mL chlorobenzene solution on quartz substrate; [c]Red-shift of the low-energy absorption peaks from solution to film; [d]Optical bandgap (estimated from the absorption onset of the polymer film); [e]Calculated from $E_{LUMO} = -e(E_{on}^{red} + 4.38)$ (eV) and $E_{HOMO} = -e(E_{on}^{ox} + 4.38)$ (eV); [f]Electrochemical band gap is derived from E_{HOMO} subtracting E_{LUMO}.

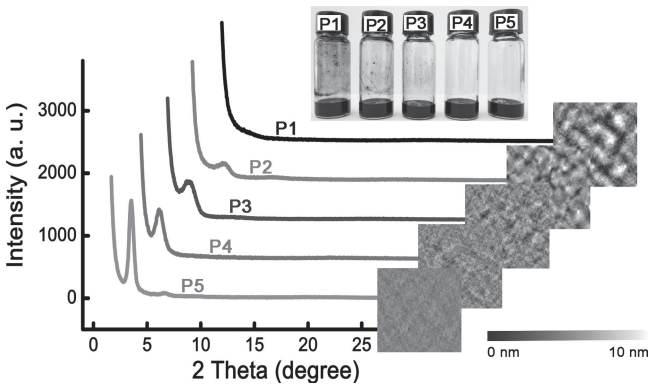

Figure 2. The out-of-plane X-ray diffraction diagrams and AFM height images (2 μm × 2 μm) of the polymer films spin-coated on quartz substrate. Inset shows photographs of each polymer in CB with a concentration of 10 mg/mL.

even opposite.[55,56] In our work, the availability of polymers with 0–100% side-chain content allows for investigation into correlation between the polymer properties and film morphology that may be altered only by side chains and the device performance such as photoresponse, dark current and detectivity of polymer photodetectors. The photodetectors were firstly fabricated with a basic structure of ITO/PEDOT:PSS/active layer/Al. The active layer is comprised of one of **P1**-**P5** and (6,6)-phenyl C_{61} butyric acid methyl ester (PCBM) in a weight ratio of 1:2. The dark current density-voltage (*J*–*V*) characteristics under reverse and forward biases (Figure S5) indicate that the devices appear to have asymmetry characteristics.[57] The dark current decreases in order of **P1** to **P5**, which apparently correlates to polymer solubility, film roughness or the numbers of side chains in polymers. The spectral profiles between the absorption spectra and external quantum efficiency (EQE) of the devices (SI) match well, indicating that the photons absorbed by the polymers in the visible to NIR spectral region contribute to the photocurrent generation.

The figure of merit of a photodetector is defined by specific detectivity (*D**). Assuming that the shot noise from the dark current is a major contributor to the noise,[35,58–60] the specific detectivity can be expressed as:

$$D^* = R/(2qJ_d)^{1/2} = (J_{ph}/J_{light})/(2qJ_d)^{1/2} \quad (1)$$

where R is the responsivity, a ratio of photocurrent (J_{ph}) to incident-light intensity (J_{light}), q is the absolute value of electron charge (1.6×10^{-19} Coulombs), and J_d is the dark current. The devices based on all the polymers exhibited photovoltaic response from 400 to 1200 nm and high responsivity in the spectral regions of 400–500 nm and 700–900 nm where these polymers also absorb intensely (**Figure 3**a). The photo-response at the short wavelength increases with an increase in side-chain content from **P1** to **P5**, which appears to correlate with the weight ratio of polymer (excluding the side chains) and PCBM. As shown in Figure 3b, spectral responsivity of the basic device with **P3** is dependent on the applied bias (0, –0.1, –0.5 and –2.0 V), which is probably due to the field-induced exciton dissociation.[60,61] Similarly, spectral responsivity of the devices based on other polymers is dependent on electric field (Figure S7). The specific detectivity of the basic devices based on **P1**-**P5** is calculated to be 10^{10}–10^{12} Jones in a broad spectral range of 400–1000 nm (Figure 3c). Variation in the detectivity is

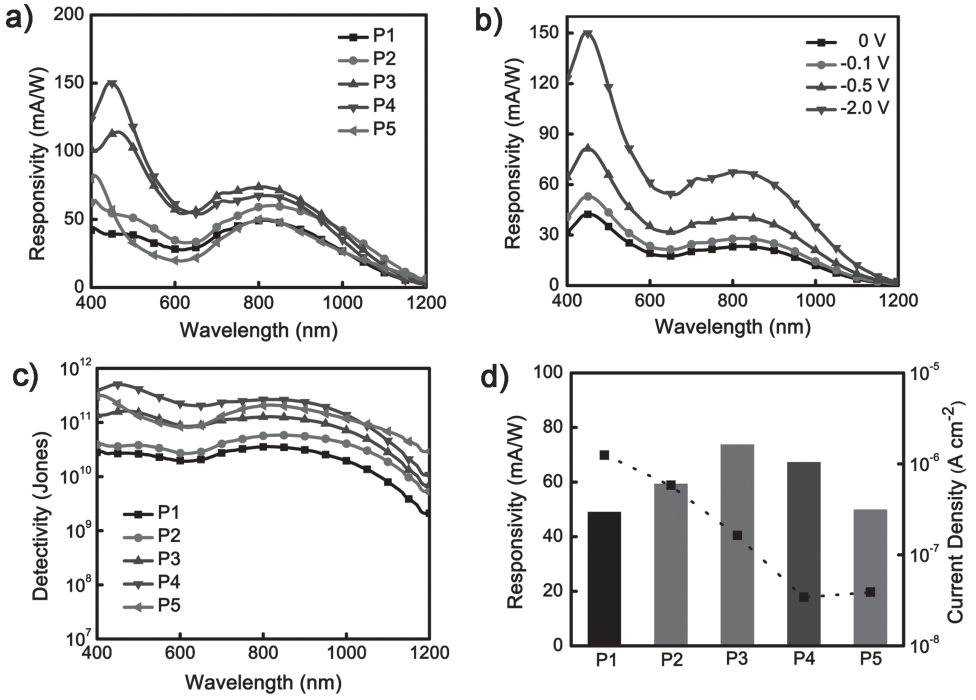

Figure 3. a) Spectral responsivity of the basic device based on **P1**-**P5** under a voltage of –2 V. b) Spectral responsivity of the basic device based on **P4** at different applied voltages. c) Specific detectivity as a function of wavelength of the basic devices based on **P1**-**P5** under a voltage of –0.1 V. d) Responsivity (color strip) at 800 nm under –2 V and the dark current density (black square) under –0.1 V of the basic device for each polymer.

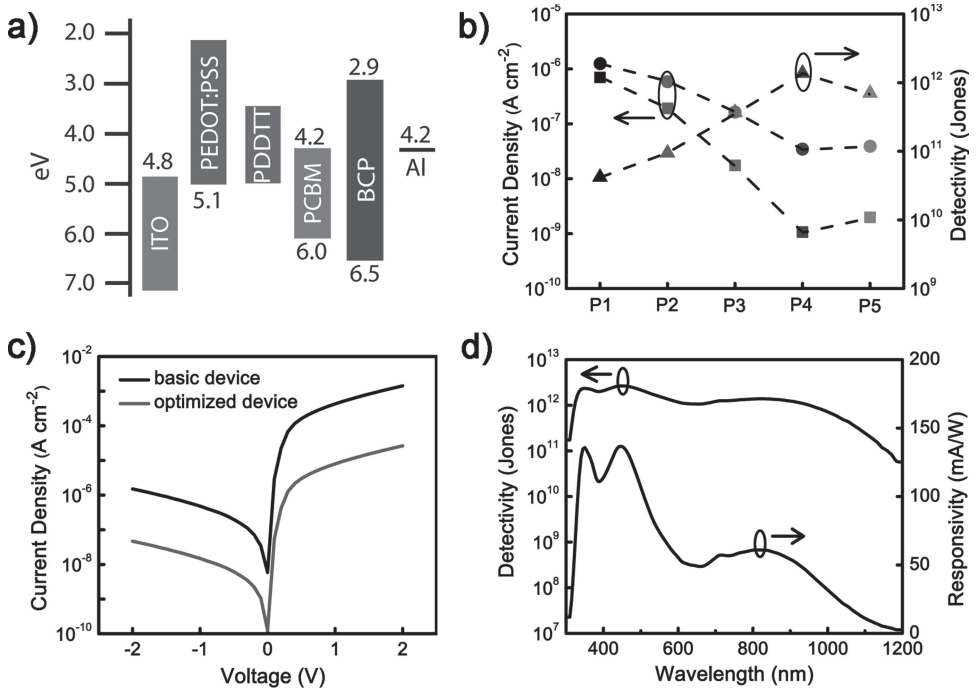

Figure 4. a) Schematic energy-level diagrams of the optimized photodetector showing efficient exciton dissociation of the active layer materials and the hole blocking effect of BCP layer. b) Specific detectivity (up triangle) at 800 nm under –0.1 V of the optimized device for each polymers, and the dark current density of the basic device (circle) and optimized device (square) under –0.1 V for each polymer. c) Current density-voltage (*J*–*V*) characteristics measured in the dark and d) spectral detectivity (–0.1 V)/responsivity (–2 V) of the optimized device with **P4**.

mainly governed by dark current, which in turn relates to the polymer, film morphology and quality and device configuration (Figure 3d). Apparently, the dark current of devices with a configuration of ITO/PEDOT:PSS/active layer/Al is relatively high, which is known to adversely affect the device performance.[36,62]

In order to reduce the dark current and improve the signal-to-noise ratio, we further optimized the photodetectors by introducing a thin layer (10 nm) of 2,9-dimethyl-4,7-diphenyl-1,10-phenanthroline (BCP) between the active layer and Al electrode, with a device structure of ITO/PEDOT:PSS/active layer/BCP/Al (optimized device). BCP is commonly used as a hole blocking layer (HBL) due to its low HOMO energy level (–6.5 eV, **Figure 4**a).[63–65] It was found that the dark current decreased significantly in 1–2 order of magnitude after the introduction of BCP layer. It is worth noting that going from **P1** to **P5**, the dark current of the corresponding devices drops more in the same order (Figure 4b). This trend can be related to the surface roughness of the active layers or polymer solubility, which is also related to the content of side chains in polymers. The AFM study clearly shows the BCP layer (10 nm) can cover the entire surface of active layer if it is smooth but not so for a rough surface (Figure S13). As a consequence, BCP is able to work fully for hole blocking in the devices with smooth active layers made of **P3**-**P5**. A slight decrease of 5–15% in EQE was found due to the reason that BCP will block the photocurrent mildly. Accordingly, the photodetector based on **P4** with 63% side-chain content exhibited the best performance among all, having the specific detectivity in order of 10^{12} Jones in the spectral range of 330–950 nm (Figure 4d).

Structurally analogous polymers **P1**-**P5** have the same main-chain structure and are only different in the amount of dodecyl side chains. It is such a small difference in side chain results in changes in the photodetector performance (**Table 3**). The photodetectors based on **P1** and **P2** show relatively lower detectivity,

Table 3. Photodetector Properties of the Basic and Optimized Devices.

polymer	Basic Device			Optimized Device		
	R [mA/W][a)]	J_d [A/cm^2][b)]	*D** [Jones][b)]	*R* [mA/W][a)]	J_d [A/cm^2][b)]	*D** [Jones][b)]
P1	49.0	1.2×10^{-6}	3.5×10^{10}	46.5	7.0×10^{-7}	4.2×10^{10}
P2	59.0	5.8×10^{-7}	5.7×10^{10}	54.5	1.9×10^{-7}	9.4×10^{10}
P3	73.7	1.6×10^{-7}	1.3×10^{11}	67.1	1.8×10^{-8}	3.7×10^{11}
P4	67.3	3.4×10^{-8}	2.6×10^{11}	60.8	1.1×10^{-9}	1.4×10^{12}
P5	49.9	3.9×10^{-8}	2.1×10^{11}	43.8	2.2×10^{-9}	7.1×10^{11}

[a)]Responsivity at 800 nm at –2 V; [b)]Dark current density and specific detectivity at 800 nm at –0.1 V.

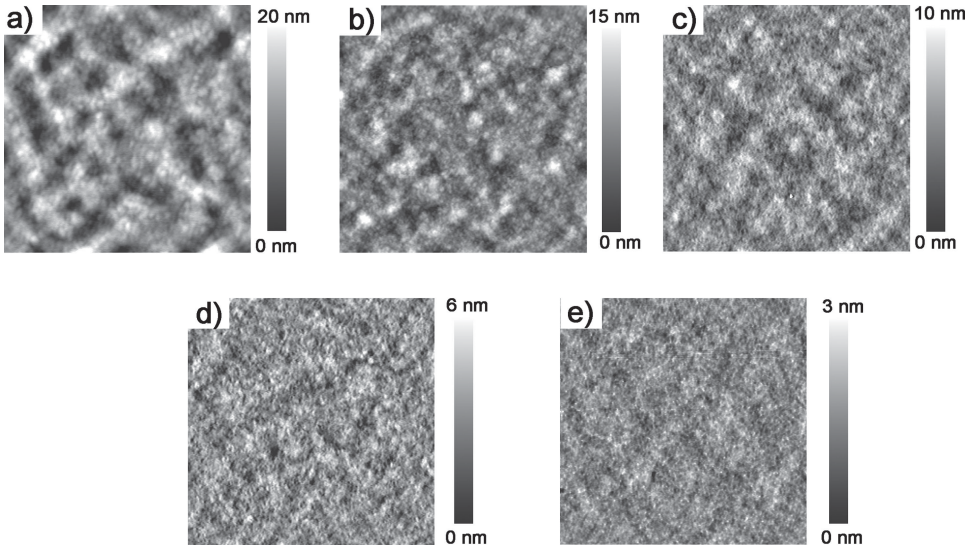

Figure 5. AFM topography images (2 μm × 2 μm) of the active layers spin-coated on glass/ITO/PEDOT:PSS.

primarily caused by the high dark current. The other three polymers with higher side-chain content (>50%) exhibit better device performance, mainly attributed to good responsivity and low dark current.[62] Among all, the optimized device based on **P4** attains the best combination of high responsivity and low dark current.

2.5. Active Layer Morphology

The appropriate morphology of active layer, particularly with regards to the optimized domain size, is critical for achieving high performance in polymer photovoltaic cells and photodetectors.[45,65,66] Since polymer side-chains are expected to impact the solubility and miscibility with PCBM, the film morphology should also be affected by the side chains.[8] Accordingly, we investigated the morphological differences of the **P1**-**P5**:PCBM films by tapping-mode AFM. As shown in **Figure 5**, the surface roughness becomes less from **P1** to **P5**. The AFM topographic images of the **P1**/**P2**:PCBM films (Figure 5a,b) reveal the formation of large and unconnected grains, which is expected to result in inefficient exciton separation and charge transport, as evident by the observed low EQE. In contrast, the surface morphology of **P3**/**P4**:PCBM films (Figure 5c,d) shows much smaller domains and fine structures with the bicontinuous interpenetrating network, which is ideal for high photoresponse and low dark current.[45,66] However, the **P5**:PCBM film (Figure 5e) exhibits a smooth and almost featureless surface with poorly defined domains and non-optimal phase segregation, which is usually not ideal for charge transport. Typically, a small domain size of about 20 nm is deemed to be essential for the exciton diffusion. The larger domains will prevent efficient exciton separation, while much smaller ones will result in increased charge carrier recombination.[67] Accordingly, the **P4**:PCBM film has the most favorable morphology for exciton dissociation, which is attributed to the high responsivity and low dark current in the corresponding device.[66,68] These results suggest that **P4** presents the most adequate combination of solubility and miscibility with PCBM to achieve optimal film morphology.

3. Conclusion

We have demonstrated a molecular engineering approach to the optimization of desired processability, molecular stacking and film property by fine tuning the side chain structure of the thienothiadiazole-based low-bandgap polymers. By adjusting the side-chain content of a series of analogous polymers, the structure-property relationship is established and polymer **P4** with 63% of side-chain content is identified as an ideal material for use in photodetector. Polymer **P4**-based photodetector shows specific detectivity of about 10^{12} Jones in the spectral range of 330–950 nm, which is among the best reported values for polymer photodetectors and even comparable to the silicon photodetector.

4. Experimental Section

Materials: All the chemicals and reagents were used as received from commercial sources without any purification. Solvents for chemical synthesis were purified by distillation. Chemical reactions were carried out under an argon atmosphere. Detailed syntheses and characterizations of the monomers and polymers are given in SI.

Characterizations: The ^{1}H (400 MHz) and ^{13}C (100 MHz) nuclear magnetic resonance (NMR) spectra were recorded using a Bruker Avance 400 NMR spectrometer using deuterated chloroform as the solvent. The high-temperature ^{1}H NMR spectra (400 MHz) of the polymers were recorded using deuterated tetrachloroethane (TCE-d_2) as the solvent at a temperature of 120 °C. Tetramethylsilane (TMS) was used as internal reference for the NMR analyses. Matrix-assisted laser desorption ionization time-of-flight mass spectrometry (MALDI-TOF MS) was obtained from Bruker Daltonics Autoflex III TOF/TOF. Elemental analysis was performed on a FlashEA1112 Elementar Analysis

Instrument. Gel permeation chromatography (GPC) analysis was conducted on a PL-GPC 220 system with polystyrene as standard and 1,2,4-trichlorobenzene as eluent at 150 °C. Cyclic voltammetry (CV) was performed on a CHI660b electrochemical workstation in a solution of n-Bu_4NPF_6 (0.1 M) in dry acetonitrile with a scan rate of 50 mV/s at room temperature under argon. A Pt disk (2 mm diameter) was used as the working electrode with a Pt wire as the counter electrode and an Ag/AgCl electrode as the reference electrode. The redox potentials were calibrated by using ferrocene as an internal standard. Thermogravimetric analysis (TGA) measurements were performed on a PerkinElmer Thermal Analysis Instruments Pyris Diamond TG from 50 to 800 °C at a heating rate of 10 °C/min under a continuous nitrogen flow. Differential scanning calorimetry (DSC) measurements were performed on a TA-DSC Q100 (TA Instruments from 20 to 250 °C at a heating rate of 10 °C/min under a continuous nitrogen flow). The UV–Vis–NIR absorption spectra were recorded on a Shimadzu UV-3600 spectrophotometer at room temperature. Atomic Force Microscopy (AFM, SPA 300HV with a SPI 3800N Probe Station, Seiko Instruments Inc., Japan) studies were carried out in room-temperature air. The probes were FORTA probes from Applied Nanostructures, which had a silicon cantilever of nominal spring constant of 2.0 N/m, a nominal resonance frequency of ~70 kHz, and were tuned to a RMS cantilever oscillation amplitude of ~1000 mV. Acquired images of 2 μm were taken with a scan frequency of 0.8 Hz. X-ray diffraction (XRD) measurements were performed on a D8 Focus diffractometer at a scan rate of 0.6° min^{-1} in the 2θ range from 2° to 35° with graphite-monochromated Cu Kα radiation (λ = 0.15405 nm). The polymer films were prepared by spin-casting chlorobenzene solutions (10 mg/mL) onto quartz substrates.

Polymerization: Representative procedure for the Stille-coupling polymerization of **P3**: A 50 mL Schlenk tube was heated under reduced pressure and then allowed to cool to room temperature under argon. In this tube, 2,5-bis(5-bromo-3-dodecyl-2-thienyl) thieno[3,4-*b*][1,2,5]thiadiazole (monomer **1**) (240.3 mg, 0.3 mmol), 2,5-bis(trimethylstannyl) thiophene (monomer **2**) (61.5 mg, 0.15 mmol) and 2,5-bis(trimethylstannyl)-3,4-bisdodecyl thiophene (monomer **3**) (112.0 mg, 0.15 mmol) were dissolved in dry chlorobenzene (15 mL) and degassed with argon for 30 min. $Pd_2(dba)_3$ (10 mg) and P(o-tolyl)$_3$ (40 mg) were then added to the reaction mixture under argon and degassed, filled with argon several times. The reaction mixture was stirred vigorously at 120 °C for 72 h under argon. Then 2-bromothiophene (30 mg, 0.2 mmol) was added and the reaction was continued for another 12 h. After cooling down to 80 °C, aqueous solution of **s**odium diethyldithiocarbamate trihydrate was added to remove the residual palladium catalyst. After 12 h, the mixture was poured into water and extracted with chlorobenzene. The combined organic layers were washed with pure water several times and dried over anhydrous $MgSO_4$. The polymer solution was concentrated to approximately 20 mL, the mixture was poured and stirred into 200 mL of methanol for 4 h, filtered and then extracted on a Soxhlet's extractor with acetone, hexane, chloroform or chlorobenzene successively. The final product was obtained by precipitating the concentrated chloroform or chlorobenzene solution into methanol. The polymer was collected by filtration and dried under reduced pressure at room temperature for at least 24 h to obtain a black solid, 231 mg (86% yield). ^{1}H NMR (400 MHz, $C_2D_2Cl_4$, 120 °C) δ (ppm): 6.87–7.59 (m, 3H), 2.36–3.29 (m, 6H), 1.17–2.09 (m, 60H), 1.00 (br, 9H). (C52H80N2S5)n (893.53): Calcd. C, 69.90; H, 9.02; N, 3.14; S, 17.94. Found C, 69.73; H, 8.96; N, 3.19; S, 18.12. GPC M_n = 13.6 kDa, M_w = 20.2 kDa; PDI = 1.49.

Fabrication of Photodetectors: A mixture of a given polymer and [6,6]-phenyl-C_{61}-butyric acid methyl ester (P_{61}CBM, ADS61BFB) in a weight ratio of 1:2 was dissolved in chlorobenzene with a total concentration of 24 mg/mL and stirred under nitrogen atmosphere at 60 °C for more than 12 h. For device fabrication, Indium tin oxide (ITO) coated glass substrates were cleaned, sequentially, by ultrasonic treatment in detergent, de-ionized water, acetone and isopropyl alcohol. A conducting film of PEDOT:PSS (Baytron P VP A1 4083) was spin-coated at 3500 rpm for 60 s after UV-plasma treatment of ITO-coated slides for 15 min, followed by annealing at 120 °C for 30 min, forming a film of about 30 nm thickness. The active layer solution was spin-coated at a speed of 1000 rpm for 60 s to get a film of 120-nm thickness. BCP and Al electrode were deposited by thermal evaporation. The active device area is 16 mm^2, which is defined by shadow masks.

Characterization of Photodetectors: All the measurements were carried out under ambient conditions. For quantum efficiency measurements, a setup made by Beijing 7-Star Optical Instruments Co., Ltd was used. Incident light from a halogen lamp (250 W) passing through a monochromator was chopped at 160 Hz and focused on the active area of the device. The photodetector signal was first amplified using a low-noise current amplifier (DLPCA-200, Femto) and then detected with a lock-in amplifier (SR830, Stanford Research Systems). Reverse bias on the device was provided by a Keithley 236 Source Measure Unit. A crystalline silicon diode (S1337–1010BQ, Hamamatsu) calibrated by the National Institute of Metrology of China was used as a reference before each measurement.

Supporting Information

Supporting Information is available from the Wiley Online Library or from the author.

Acknowledgements

This work was supported by National Natural Science Foundation of China (21134005, 21474102 and 21474105) and the Natural Science and Engineering Research Council of Canada.

Received: June 13, 2014
Revised: August 27, 2014
Published online: September 30, 2014

[1] A. C. Grimsdale, K. L. Chan, R. E. Martin, P. G. Jokisz, A. B. Homlmes, *Chem. Rev.* **2009**, *109*, 897.
[2] M. Muccini, *Nat. Mater.* **2006**, *5*, 605.
[3] S. Günes, H. Neugebauer, N. S. Sariciftci, *Chem. Rev.* **2007**, *107*, 1324.
[4] H. Dong, H. Zhu, Q. Meng, X. Gong, W. Hu, *Chem. Soc. Rev.* **2012**, *41*, 1754.
[5] Y. Li, *Acc. Chem. Res.* **2012**, *45*, 723.
[6] Y. Huang, X. Guo, F. Liu, L. Huo, Y. Chen, T. P. Russell, C. C. Han, Y. Li, J. Hou, *Adv. Mater.* **2012**, *24*, 3383.
[7] W. Li, W. S. C. Roelofs, M. M. Wienk, R. A. J. Janssen, *J. Am. Chem. Soc.* **2012**, *134*, 13787.
[8] A. T. Yiu, P. M. Beaujuge, O. P. Lee, C. H. Woo, M. F. Toney, J. M. J. Fréchet, *J. Am. Chem. Soc.* **2012**, *134*, 2180.
[9] I. Osaka, M. Saito, T. Koganezawa, K. Takimiya, *Adv. Mater.* **2014**, *26*, 331.
[10] J.-H. Dou, Y.-Q. Zheng, T. Lei, S.-D. Zhang, Z. Wang, W.-B. Zhang, J.-Y. Wang, J. Pei, *Adv. Funct. Mater.* **2014**, DOI: 10.1002/adfm.201401822.
[11] C. Cui, W.-Y. Wong, Y. Li, *Energy Environ. Sci.* **2014**, *7*, 2276.
[12] T. Lei, J.-Y. Wang, J. Pei, *Chem. Mater.* **2014**, *26*, 594.
[13] P. F. Moonen, I. Yakimets, J. Huskens, *Adv. Mater.* **2012**, *24*, 5526.
[14] F. C. Krebs, *Sol. Energy Mater. Sol. Cells* **2009**, *93*, 394.
[15] Y. J. Cheng, S. H. Yang, C. S. Hsu, *Chem. Rev.* **2009**, *109*, 5868.
[16] P.-L. T. Boudreault, A. Najari, M. Leclerc, *Chem. Mater.* **2011**, *23*, 456.
[17] J. Mei, Z. Bao, *Chem. Mater.* **2014**, *26*, 604.
[18] Z. Li, S.-W. Tsang, X. Du, L. Scoles, G. Robertson, Y. Zhang, F. Toll, Y. Tao, J. Lu, J. Ding, *Adv. Funct. Mater.* **2011**, *21*, 3331.

[19] Y. Deng, Y. Chen, J. Liu, L. Liu, H. Tian, Z. Xie, Y. Geng, F. Wang, *ACS Appl. Mater. Interfaces* **2013**, *5*, 5741.
[20] B. Fu, J. Baltazar, A. R. Sankar, P.-H. Chu, S. Zhang, D. M. Collard, E. Reichmanis, *Adv. Funct. Mater.* **2014**, *24*, 3734.
[21] J. Lee, M. Kim, B. Kang, S. B. Jo, H. G. Kim, J. Shin, K. Cho, *Adv. Energy Mater.* **2014**, *4*, 1400087.
[22] N. Blouin, A. Michaud, D. Gendron, S. Wakim, E. Blair, R. Neagu-Plesu, M. Belletête, G. Durocher, Y. Tao, M. Leclerc, *J. Am. Chem. Soc.* **2008**, *130*, 732.
[23] Y. Zou, A. Najari, P. Berrouard, S. Beaupré, B. R. Aïch, Y. Tao, M. Leclerc, *J. Am. Chem. Soc.* **2010**, *132*, 5330.
[24] H. Zhou, L. Yang, A. C. Stuart, S. C. Price, S. Liu, W. You, *Angew. Chem.* **2011**, *123*, 3051.
[25] Y. Liang, D. Feng, Y. Wu, S.-T. Tsai, G. Li, C. Ray, L. Yu, *J. Am. Chem. Soc.* **2009**, *131*, 7792.
[26] B. Kim, X. Ma, C. Chen, Y. Ie, E. W. Coir, H. Hashemi, Y. Aso, P. F. Green, J. Kieffer, J. Kim, *Adv. Funct. Mater.* **2013**, *23*, 439.
[27] C. Cabanetos, A. E. Labban, J. A. Bartelt, J. D. Douglas, W. R. Mateker, J. M. J. Fréchet, M. D. McGehee, P. M. Beaujuge, *J. Am. Chem. Soc.* **2013**, *135*, 4656.
[28] L. Huo, S. Zhang, X. Guo, F. Xu, Y. Li, J. Hou, *Angew. Chem. Int. Ed.* **2011**, *50*, 9697.
[29] L. Fang, Y. Zhou, Y.-X. Yao, Y. Diao, W.-Y. Lee, A. L. Appleton, R. Allen, J. Reinspach, S. C. B. Mannsfeld, Z. Bao, *Chem. Mater.* **2013**, *25*, 4874.
[30] V. Kamm, G. Battagliarin, I. A. Howard, W. Pisula, A. Mavrinskiy, C. Li, K. Müllen, F. Laquai, *Adv. Energy Mater.* **2011**, *1*, 297.
[31] I. Osaka, T. Kakara, N. Takemura, T. Koganezawa, K. Takimiya, *J. Am. Chem. Soc.* **2013**, *135*, 8834.
[32] T. E. Kang, H.-H. Cho, H. jun Kim, W. Lee, H. Kang, B. J. Kim, *Macromolecules* **2013**, *4*, 6806.
[33] C. L. Chochos, S. A. Choulis, *Prog. Polym. Sci.* **2011**, *36*, 1326.
[34] S. K. Son, Y.-S. Kim, H. J. Son, M. J. Ko, H. Kim, D.-K. Lee, J. Y. Kim, D. H. Choi, K. Kim, B. S. Kim, *J. Phys. Chem. C* **2014**, *118*, 2237.
[35] X. Gong, M. Tong, Y. Xia, W. Cai, J. S. Moon, Y. Cao, G. Yu, C.-L. Shieh, B. Nilsson, A. J. Heeger, *Science* **2009**, *325*, 1665.
[36] J. D. Yuen, R. Kumar, J. Seifter, S. Valouch, D. Zakhidov, D. Moses, U. Lemmer, A. J. Heeger, F. Wudl, *J. Am. Chem. Soc.* **2011**, *133*, 19602.
[37] K.-J. Baeg, M. Binda, D. Natali, M. Caironi, Y.-Y. Noh, *Adv. Mater.* **2013**, *25*, 4267.
[38] G. Azzellino, A. Grimoldi, M. Binda, M. Caironi, D. Natali, M. Sampietro, *Adv. Mater.* **2013**, *25*, 6829.
[39] K. K. Manga, S. Wang, M. Jaiswal, Q. Bao, K. P. Loh, *Adv. Mater.* **2010**, *22*, 5265.
[40] P. M. Beaujuge, J. M. J. Fréchet, *J. Am. Chem. Soc.* **2011**, *133*, 20009.
[41] Y. Deng, J. Liu, J. Wang, L. Liu, W. Li, H. Tian, X. Zhang, Z. Xie, Y. Geng, F. Wang, *Adv. Mater.* **2014**, *26*, 471.
[42] T.-Ya. Chu, J. Lu, S. Beaupré, Y. Zhang, J.-R. Pouliot, J. Zhou, A. Najari, M. Leclerc, Y. Tao, *Adv. Funct. Mater.* **2012**, *22*, 2345.
[43] Z. Li, J. Ding, N. Song, X. Du, J. Zhou, J. Lu, Y. Tao, *Chem. Mater.* **2011**, *23*, 1977.
[44] Q. Shi, H. Fan, Y. Liu, J. Chen, L. Ma, W. Hu, Z. Shuai, Y. Li, X. Zhan, *Macromolecules* **2011**, *44*, 4230.
[45] M. Seri, M. Bolognesi, Z. Chen, S. Lu, W. Koopman, A. Facchetti, M. Muccini, *Macromolecules* **2013**, *46*, 6419.
[46] B. Sun, W. Hong, Z. Yan, H. Aziz, Y. Li, *Adv. Mater.* **2014**, *26*, 2636.
[47] J. Huang, Y. Zhao, W. He, H. Jia, Z. Lu, B. Jiang, C. Zhan, Q. Pei, Y. Liu, J. Yao, *Polym. Chem.* **2012**, *3*, 2832.
[48] P. W. M. Blom, V. D. Mihailetchi, L. J. A. Koster, D. E. Markov, *Adv. Mater.* **2007**, *19*, 1551.
[49] L. Huo, L. Ye, Y. Wu, Z. Li, X. Guo, M. Zhang, S. Zhang, J. Hou, *Macromolecules* **2012**, *45*, 6923.
[50] J. W. Jung, F. Liu, T. P. Russell, W. H. Jo, *Energy Environ. Sci.* **2013**, *6*, 3301.
[51] L. Dou, C.-C. Chen, K. Yoshimura, K. Ohya, W.-H. Chang, J. Gao, Y. Liu, E. Richard, Y. Yang, *Macromolecules* **2013**, *46*, 3384.
[52] S. Loser, C. J. Bruns, H. Miyauchi, R. P. Ortiz, A. Facchetti, S. I. Stupp, T. J. Marks, *J. Am. Chem. Soc.* **2011**, *133*, 8142.
[53] G. K. Dutta, A.-R. Han, J. Lee, Y. Kim, J. H. Oh, C. Yang, *Adv. Funct. Mater.* **2013**, *23*, 5317.
[54] J. D. Yuen, R. Kumar, D. Zakhidov, J. Seifter, B. Lim, A. J. Heeger, F. Wudl, *Adv. Mater.* **2011**, *23*, 3780.
[55] C. Piliego, T. W. Holcombe, J. D. Douglas, C. H. Woo, P. M. Beaujuge, J. M. J. Fréchet, *J. Am. Chem. Soc.* **2010**, *132*, 7595.
[56] J. D. Azoulay, Z. A. Koretz, B. M. Wong, G. C. Bazan, *Macromolecules* **2013**, *46*, 1337.
[57] X. Liu, H. Wang, T. Yang, W. Zhang, X. Gong, *ACS Appl. Mater. Interfaces* **2012**, *4*, 3701.
[58] Y. Xie, M. Gong, T. A. Shastry, J. Lohrman, M. C. Hersam, S. Ren, *Adv. Mater.* **2013**, *25*, 3433.
[59] G. Qian, J. Qi, J. A. Davey, J. S. Wright, Z. Y. Wang, *Chem. Mater.* **2012**, *24*, 2364.
[60] R. Saran, M. N. Nordin, R. J. Curry, *Adv. Funct. Mater.* **2013**, *23*, 4149.
[61] D. Yang, X. Zhou, D. Ma, *Org. Electron.* **2013**, *14*, 3019.
[62] E. Saracco, B. Bouthinon, J.-M. Verilhac, C. Celle, N. Chevalier, D. Mariolle, O. Dhez, J.-P. Simonato, *Adv. Mater.* **2013**, *25*, 6534.
[63] F. Guo, B. Yang, Y. Yuan, Z. Xiao, Q. Dong, Y. Bi, J. Huang, *Nat. Nanotechnol.* **2012**, *7*, 798.
[64] F. Guo, Z. Xiao, J. Huang, *Adv. Opt. Mater.* **2013**, *1*, 289.
[65] J. Qi, L. Ni, D. Yang, X. Zhou, W. Qiao, M. Li, D. Ma, Z. Y. Wang, *J. Mater. Chem. C* **2014**, *2*, 2431.
[66] P. E. Keivanidis, P. K. H. Ho, R. H. Friend, N. C. Greenham, *Adv. Funct. Mater.* **2010**, *20*, 3895.
[67] J. Peet, A. J. Heeger, G. C. Bazan, *Acc. Chem. Res.* **2009**, *42*, 1700.
[68] X. Liu, H. Wang, T. Yang, W. Zhang, I.-F. Hsieh, S. Z. D. Cheng, X. Gong, *Org. Electron.* **2012**, *13*, 2929.